# Safety Measures for VTOL UAV Lifting a Cable-Suspended Load with Unexpected Mass

Henrik Söderlund

Department of Applied Physics and Electronics
Umeå University, Sweden
henrik.soderlund@umu.se

**Abstract.** Among the causes of helicopter lifting accidents, some of the most hazardous conditions are induced swing of the payload as it clears the ground and overloading the helicopter. This paper evaluates the need for safety measures during payload lifting when the suspended load mass is unexpectedly large or small. A state machine is proposed together with two safety measures and an update routine for estimating the true mass if it differs from the assumed mass. Trajectory control with maintained tension on the cable is proposed and the method is shown to be reliable. The safety measures proposed seem to be valuable additions to the lifting maneuver.

## 1 Introduction

The field of aerial robotics, especially multi-rotor unmanned aerial vehicles (UAVs) has seen a major increase in attendance during the last decade. With the rise of high-performance micro-scale processing units and high-precision sensors, flying robots have become more desired commercially [1]. Multi-rotor aerial vehicles allow for vertical take-off and landing (VTOL) while also being capable of agile maneuvering. Because of this, VTOL UAVs are an attractive alternative for transporting light-weight cargo over untraversable terrains [2].

Extensive research has gone into trajectory control for multi-rotor aerial vehicles transporting cable-suspended payloads [3, 4, 5]; from adaptive controllers for unknown mass scenarios and trajectory generation for swing-free maneuvers to cooperative lifting using multiple aerial vehicles. The problem of payload lifting seem to be a subject left out by most research, but is a valid subject to investigate further in the field of UAV transportation [2].

Among the causes of helicopter lifting accidents, some of the hazardous conditions are overloading the helicopter and injuries caused by loads swinging as they first clear the ground. Because of the dangers a swinging massive object can pose on the surroundings, the aerial vehicle has to be straight above the load before the helicopter starts to lift according to safety regulations for helicopter lifting, Ontario, Canada [6].

From the point where the aerial vehicle with a cable-suspended load lifts with the cable slacking to when it becomes taut, the VTOL UAV experiences

switching dynamics. This is why both dynamics of a multi-rotor UAV without a suspended load and dynamics with a suspended load have to be considered. Cruz et al. [2] proposes a mathematical model of a quadrotor with a cable-suspended load combined with trajectory generation and control laws for performing such lift maneuvers while minimizing swing of the cable-suspended load at the moment of lift-off. According to [6], it is critical to know accurate load weights and sizes since each helicopter has a limited lifting capacity. When the cargo weight has been mislabeled, the consequences could be hazardous, especially if the load mass is unexpectedly too small. Therefore, the methods proposed by [2] could be extended by implementing safety measures to test and compensate for unexpected deviations of the load mass and for when the load weight exceeds the aerial vehicle load capacity.

### 1.1 Objective

This paper evaluates the need for safety measures in the switching dynamics of the system when the suspended load mass is unexpectedly large or small. A new safety mechanism will be introduced in the form of a procedure for carefully testing the load mass, which extends the proposal of a lifting maneuver made by [2]. The robustness and accuracy of the procedure will be analyzed and discussed upon.

## 2 Theory

The typical mathematical model for a multi-rotor aerial vehicle with four rotors will be introduced based on Mahony et al. [7] and Bouabdallah et al. [8]. Then, dynamical models for a multi-rotor UAV with a cable-suspended load during different stages will be introduced using Cruz et al. [2]. Moreover, the concept of *cable collision* will be covered from what is proposed by Bisgaard et al. [9].

### 2.1 Quadrotor Model

The multi-rotor design allows the UAV to be kept stabilized in air and steered freely in all directions. We will focus mainly on the quadrotor as a reference model. As shown in Fig. 1, the quadrotor comprises two pairs of rotors that are on the opposite sides of each other. Each rotor pair rotates in the same direction, but in the opposite direction of the other rotor pair. By applying inequal thrust to the pairs of rotating rotors corresponding to the direction of rotation, one can control pitch and roll. Yaw rotation can be controlled by adjusting the average speed of the rotor pairs individually.The total thrust is controlled by increasing or decreasing the average thrust of all rotors in the same amount [7].

Let $\{E\}$ denote the inertial frame with unit vectors along the axes denoted by $\{\boldsymbol{x}_E,\ \boldsymbol{y}_E,\ \boldsymbol{z}_E\}$ and $\{B\}$ denote the body fixed frame for the quadrotor with unit vectors along the axes denoted by $\{\boldsymbol{x}_B,\ \boldsymbol{y}_B,\ \boldsymbol{z}_B\}$ as illustrated in Fig. 1. We

can relate the frames with three Z-X-Y Euler angles to form a rotation matrix. The rotation matrix $\boldsymbol{R}$ of the quadrotor to get from $\{E\}$ to $\{B\}$ is defined as [7]

$$\boldsymbol{R} = \begin{pmatrix} c_\psi\, c_\theta & s_\phi\, s_\theta\, s_\psi - c_\phi\, s_\psi & c_\phi\, s_\theta\, c_\psi + s_\phi\, s_\psi \\ s_\theta\, s_\psi & s_\phi\, s_\theta\, s_\psi + c_\theta\, c_\psi & c_\phi\, s_\theta\, s_\psi \\ -s_\theta & s_\phi\, c_\theta & c_\phi\, c_\theta \end{pmatrix} \tag{1}$$

where $c$ and $s$ are abbrevations for cosine and sine, respectively. $\psi$ is the yaw rotation about the $Z$ axis, $\phi$ is the roll rotation about the $X$ axis and $\theta$ is the pitch rotation about the $Y$ axis.

In Newton-Euler formalism, the dynamics of a rigid body under external forces applied to the center of mass and expressed in $\{B\}$ are [8]

$$\begin{pmatrix} m\boldsymbol{I}_{3\times 3} & 0 \\ 0 & \boldsymbol{I}_{x,y,z} \end{pmatrix} \begin{pmatrix} \dot{\boldsymbol{v}} \\ \dot{\boldsymbol{\Omega}} \end{pmatrix} + \begin{pmatrix} \boldsymbol{\Omega} \times m\boldsymbol{v} \\ \boldsymbol{\Omega} \times \boldsymbol{I}_{x,y,z}\boldsymbol{\Omega} \end{pmatrix} = \begin{pmatrix} \boldsymbol{F} \\ \boldsymbol{\tau} \end{pmatrix}, \tag{2}$$

where $\boldsymbol{I}_{3\times 3}$ is the $3 \times 3$ identity matrix, $\boldsymbol{I}_{x,y,z} \in \mathbb{R}^{3\times 3}$ is the constant inertia matrix, $\boldsymbol{v}$ the body linear speed vector and $\boldsymbol{\Omega}$ the body angular velocity. Based on (2) and Fig. 1, the rigid body equations of motion of the quadrotor can be written as [7] and [8]

$$\begin{cases} \dot{\boldsymbol{\rho}}_q = \boldsymbol{v}_q \\ m_q \dot{\boldsymbol{v}}_q = \boldsymbol{R}\boldsymbol{F} - m_q g \boldsymbol{z}_E \\ \dot{\boldsymbol{R}} = \boldsymbol{R}\boldsymbol{\Omega}_\times \\ \boldsymbol{I}_{x,y,z}\dot{\boldsymbol{\Omega}} = -\boldsymbol{\Omega} \times \boldsymbol{I}_{x,y,z}\boldsymbol{\Omega} + \boldsymbol{\tau} \end{cases} \tag{3}$$

where the following definitions are introduced, based on Fig. 1:

| | |
|---|---|
| $m_q \in \mathbb{R}_{>0}$ | mass of the quadrotor, |
| $g \in \mathbb{R}_{>0}$ | gravity constant, |
| $d \in \mathbb{R}_{>0}$ | distance from the central axis to each rotor support arm, respectively, |
| $\boldsymbol{I}_{x,y,z} \in \mathbb{R}^{3\times3}$ | constant inertia matrix expressed in $\{B\}$, |
| $\omega_i \in \mathbb{R}$ | angular speed of the $i$th rotor, |
| $\boldsymbol{\rho}_q, \boldsymbol{v}_q \in \mathbb{R}^3$ | position and velocity of the quadrotor center of mass in with respect to $\{E\}$, $\boldsymbol{\rho}_q = [x_q\ y_q\ z_q]^T$ and $\boldsymbol{v}_q = [\dot{x}_q\ \dot{y}_q\ \dot{z}_q]^T$, |
| $\boldsymbol{R} \in SO(3)$ | rotation matrix from $\{E\}$ to $\{B\}$, |
| $\phi \in \mathbb{R}$ | roll angle of quadrotor around $\boldsymbol{x}_B$, |
| $\theta \in \mathbb{R}$ | pitch angle of quadrotor around $\boldsymbol{y}_B$, |
| $\psi \in \mathbb{R}$ | yaw angle of quadrotor around $\boldsymbol{z}_B$, |
| $\boldsymbol{\Omega} \in \mathbb{R}^3$ | angular velocity of the quadrotor in with respect to $\{E\}$, expressed in $\{B\}$, |
| $\boldsymbol{\Omega}_\times \in \mathbb{R}^{3\times3}$ | a skew-symmetric matrix, such that $\boldsymbol{\Omega}_\times \boldsymbol{v} = \boldsymbol{\Omega} \times \boldsymbol{v}$, $\forall \boldsymbol{v} \in \mathbb{R}^3$, |
| $\boldsymbol{F} \in \mathbb{R}^3$ | total thrust produced by the quadrotor expressed in $\{B\}$, |
| $\boldsymbol{\tau} \in \mathbb{R}^3$ | net moment applied to the airframe of the quadrotor by the aerodynamics of the rotors, expressed in $\{B\}$. |

Table 1: Notation for the dynamic model of the quadrotor.

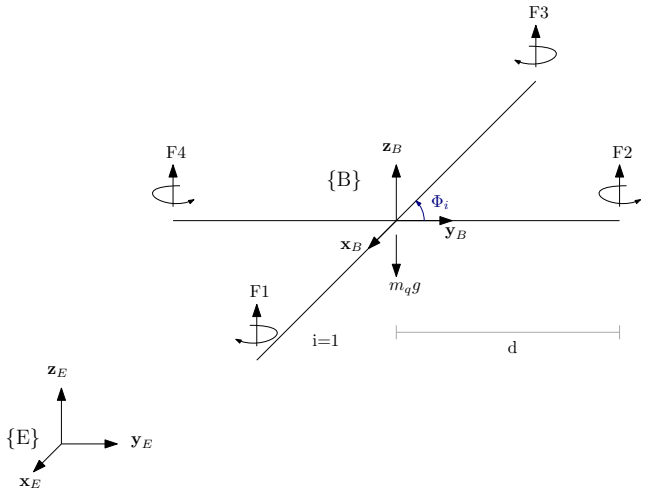


Fig. 1: Quadrotor configuration frame system without a suspended load. Introducing the fixed body frame $\{B\}$ and the inertial frame $\{E\}$.

### 2.2 Aerodynamics

For an N-rotor aerial vehicle, we denote the rotors $i \in \{1 \dots N\}$ in the direction as shown in Fig. 1. Each rotor is positioned at an angle $\Phi_i = \frac{\pi}{2}(i-1)$ between the rotor support arm and $\{B\}$. In addition to this, we introduce $\sigma_i = \{-1, +1\}$ which denotes the direction of roation for rotor $i$ [7].

In order to relate the angular speeds $\boldsymbol{\omega} = (\omega_1, \omega_2, \dots, \omega_N)$ of the rotors to the net moment $\boldsymbol{\tau} = (\tau_1, \tau_2, \tau_3)$ arising from aerodynamics, we introduce a basic aerodynamic model from [7].

The net moment $\boldsymbol{\tau}$ arising from the aerodynamics applied to the N-rotor airframe is related to the sum of angular speeds of the rotors as [7]

$$\begin{cases} \tau_1 = c_T \sum_{i=1}^{N} d_i \sin(\Phi_i) \omega_i^2 \\ \tau_2 = -c_T \sum_{i=1}^{N} d_i \cos(\Phi_i) \omega_i^2 \\ \tau_3 = c_Q \sum_{i=1}^{N} \sigma_i \omega_i^2 \end{cases} \tag{4}$$

where constants $c_T$ (related to the steady-state thrust) and $c_Q$ (related to the reaction torque) can be acquired through static thrust tests in experiment, which also includes the effect of drag on the rigid body induced by the rotor flow [7].

The hover thrust $T_\Sigma$ applied to the body is the sum of the thrusts from each individual rotor expressed as [7]

$$T_\Sigma = c_T \sum_{i=1}^{N} \omega_i^2, \tag{5}$$

which is the primary component of the total thrust vector [7]

$$\boldsymbol{F} = T_\Sigma \boldsymbol{z}_B + \boldsymbol{\Delta}. \tag{6}$$

For a quadrotor ($N = 4$), this can be expressed in matrix form as [7]

$$\begin{pmatrix} T_\Sigma \\ \tau_1 \\ \tau_2 \\ \tau_3 \end{pmatrix} = \underbrace{\begin{pmatrix} c_T & c_T & c_T & c_T \\ 0 & dc_T & 0 & -dc_T \\ -dc_T & 0 & dc_T & 0 \\ -c_Q & c_Q & -c_Q & c_Q \end{pmatrix}}_{\Gamma} \begin{pmatrix} \omega_1^2 \\ \omega_2^2 \\ \omega_3^2 \\ \omega_4^2 \end{pmatrix}, \tag{7}$$

and given the desired thrust $T_\Sigma$ and moments $\tau_1$, $\tau_2$ and $\tau_3$, we can solve for the required rotor velocities using the inverse of the constant matrix $\Gamma$. In order for the quadrotor to hover, a suitable $\boldsymbol{\omega}$ has to be chosen by inverting $\Gamma$ such that $\boldsymbol{\tau} = 0$ and $T_\Sigma = m_q g$ [7].

### 2.3 Suspended Load Model

From Fig. 2, we introduce the following definitions:

| | |
|---|---|
| $m_p \in \mathbb{R}_{>0}$ | mass of the load, |
| $T \in \mathbb{R}_{\geq 0}$ | tension on the cable, |
| $\ell \in \mathbb{R}_{>0}$ | length of the cable, |
| $\boldsymbol{\rho}_p, \boldsymbol{v}_p \in \mathbb{R}^3$ | position and velocity of the suspended load center of mass with respect to $\{E\}$, $\boldsymbol{\rho}_p = [x_p \ y_p \ z_p]^T$ and $\boldsymbol{v}_p = [\dot{x}_p \ \dot{y}_p \ \dot{z}_p]^T$, |
| $\boldsymbol{\mu} \in \mathbb{R}^3$ | the unit vector ($\|\boldsymbol{\mu}\| = 1$) from the load to the quadrotor center of mass. |

Table 2: Notation for the dynamic model of the load.

When the cable tension is nonzero, i.e. when the quadrotor is carrying the suspended load, the dynamics of the system can be written as [2]

$$\begin{cases} \dot{\boldsymbol{\rho}}_q = \boldsymbol{v}_q \\ m_q \dot{\boldsymbol{v}}_q = \boldsymbol{R}\boldsymbol{F} - m_q g \boldsymbol{z}_E - T\boldsymbol{\mu} \\ \dot{\boldsymbol{R}} = \boldsymbol{R}\boldsymbol{\Omega}_\times \\ \boldsymbol{I}_{x,y,z}\dot{\boldsymbol{\Omega}} = -\boldsymbol{\Omega} \times \boldsymbol{I}_{x,y,z}\boldsymbol{\Omega} + \boldsymbol{\tau} \\ \dot{\boldsymbol{\rho}}_p = \boldsymbol{v}_p \\ m_p \dot{\boldsymbol{v}}_p = T\boldsymbol{\mu} - m_p g \boldsymbol{z}_E \end{cases} \tag{8}$$

For this system, the quadrotor and load positions are related by [2]

$$\boldsymbol{\rho}_q = \boldsymbol{\rho}_p + \ell\boldsymbol{\mu}, \tag{9}$$

where $\boldsymbol{\mu}$ defines the direction:

$$\boldsymbol{\mu} = \frac{\boldsymbol{\rho}_q - \boldsymbol{\rho}_p}{\|\boldsymbol{\rho}_q - \boldsymbol{\rho}_p\|}. \tag{10}$$

As stated in Section 1, the system experiences switching dynamics during the lift maneuver when the cable tension $T$ goes from zero to a nonzero value. This transition is known as *cable collision* [9] and happens when the condition

$$\|\boldsymbol{\rho}_q - \boldsymbol{\rho}_p\| = \ell \tag{11}$$

holds. During cable collision the positions of the quadrotor and the load remain the same, but their change in velocity can be modeled as a perfectly inelastic collision [9]. Using the conversion of momentum, both elastic and inelastic impacts can be modelled. The relation between translational velocity before and after impact can be described by [9]

$${}^{+}\boldsymbol{v}_q = {}^{-}\boldsymbol{v}_q + \frac{\delta}{m_q}\boldsymbol{\mu}, \tag{12}$$

$${}^{+}\boldsymbol{v}_p = {}^{-}\boldsymbol{v}_p - \frac{\delta}{m_p}\boldsymbol{\mu}, \tag{13}$$

where $\delta$ is the collision impulse. The pre-superscripts ${}^{-}(\cdot)$ and ${}^{+}(\cdot)$ denote the values just before and just after the collision, respectively. The impact characterized by the relative velocity of the attachment points on the cable can be written as [9]

$$-k_e({}^{-}\boldsymbol{v}_q - {}^{-}\boldsymbol{v}_p)\,\boldsymbol{\mu} = ({}^{+}\boldsymbol{v}_q - {}^{+}\boldsymbol{v}_p)\,\boldsymbol{\mu}, \tag{14}$$

where $k_e \in [0,\ 1]$ is the elasticity constant such that $k_e = 0$ describes a perfect inelastic collision and $k_e = 1$ describes a perfect elastic collision [2]. To ensure ${}^{+}\boldsymbol{v}_q - {}^{+}\boldsymbol{v}_p = 0$, we have to model the cable collision as a perfect inelastic collision, i.e. $k_e = 0$. Substituting (12) and (13) into (14), we can solve (14) for $\delta$ to get the collision impulse as [9]

$$\delta = -m_q m_p \frac{{}^{-}\boldsymbol{v}_q\,\boldsymbol{\mu}}{m_q + m_p}. \tag{15}$$

Substituting (15) into (12) and (13), one can compute the states after the transition moment, when the condition (11) holds.

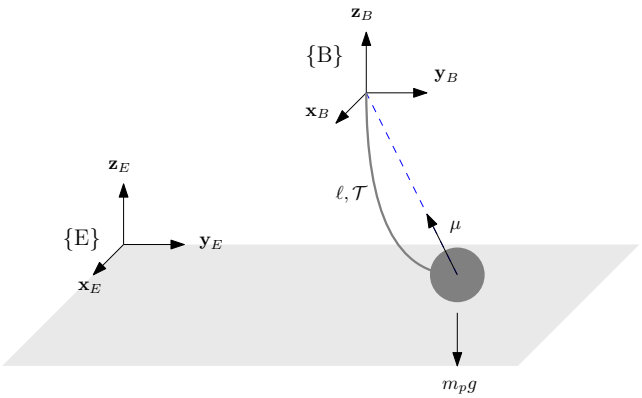


Fig. 2: Configuration frame system with a suspended load.

### 2.4 Lift Maneuver

In this section, we will follow what was found by Cruz et al. [2] quite closely. Starting with the quadrotor in a configuration similar to Fig. 2, the goal is to lift the load until it reaches a predefined height $h$. The holonomic constraint between the quadrotor and the cable-suspended load relies on the cable length $\ell$ and for simplicity, we say that this constraint can not be broken. [2, Problem 1] states that a cable-suspended load is lying on the ground at the initial position $\boldsymbol{\rho}_p^{(0)} = [x_p^{(0)} \; y_p^{(0)} \; z_p^{(0)}]^T$ which is attached to the quadrotor hovering at the position $\boldsymbol{\rho}_q^{(0)} = [x_q^{(0)} \; y_q^{(0)} \; z_q^{(0)}]^T$ such that

$$\boldsymbol{z}_p^{(0)} = \boldsymbol{\rho}_p^{(0)} \boldsymbol{z}_E = 0, \quad \|\boldsymbol{\rho}_q^{(0)} - \boldsymbol{\rho}_p^{(0)}\| < \ell, \quad \boldsymbol{z}_q^{(0)} = \boldsymbol{\rho}_q^{(0)} \boldsymbol{z}_E > 0, \tag{16}$$

where the superscript $(\cdot)^{(0)}$ indicates the intial value of a variable. The quadrotor has to lift the load until it reaches the goal position

$$\boldsymbol{\rho}_p^{(f)} = \boldsymbol{\rho}_p^{(0)} + h\boldsymbol{z}_E, \tag{17}$$

where the superscript $(\cdot)^{(f)}$ indicates the final value of a variable.

The lift maneuver is comprised of three finite states as shown in Fig. 3: *Setup*, *Pull* and *Raise*. This decomposition is due to the transition between zero to nonzero cable tension and from the load being in contact with the ground to being lifted in air [2].

- **Setup:**
  The quadrotor starts at an initial configuration according to Fig. 3a with the cable tension at zero. Due to the corresponding condition (16), the quadrotor and the suspended load can be considered as separate systems. Since the suspended load is rested on the ground, we write the total dynamics of the system in the same manner as given in (3). The equations of motion for the quadrotor at the *Setup* state can be written as

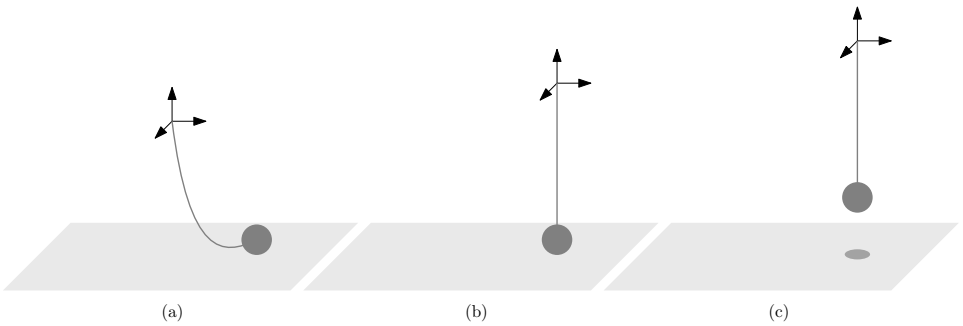


Fig. 3: Lifting states. (a) is *Setup*, (b) is *Pull* and (c) is *Raise*.

$$\begin{bmatrix} \dot{\boldsymbol{\rho}}_q \\ \dot{\boldsymbol{v}}_q \\ \dot{\boldsymbol{R}} \\ \dot{\boldsymbol{\Omega}} \end{bmatrix} = \begin{bmatrix} \boldsymbol{v}_q \\ m_q^{-1}\boldsymbol{R}\boldsymbol{F} - g\boldsymbol{z}_E \\ \boldsymbol{R}\boldsymbol{\Omega}_\times \\ \boldsymbol{I}_{x,y,z}^{-1}(-\boldsymbol{\Omega} \times \boldsymbol{I}_{x,y,z}\boldsymbol{\Omega} + \boldsymbol{\tau}) \end{bmatrix}. \tag{18}$$

– **Pull:**
The transition from *Setup* to *Pull* happens when the condition

$$\|\boldsymbol{\rho}_q - \boldsymbol{\rho}_p\| = \ell \tag{19}$$

holds, i.e. when the quadrotor and the load are exactly distanced by $\ell$ (Fig. 3b). The cable is now fully extended, which means that $\mathcal{T} \neq 0$. This does not mean that the tension is enough to lift the payload [2]. The quadrotor is affected by the tension on the cable in the direction of $\boldsymbol{\mu}$, but is constrained to a half sphere with its center at $\boldsymbol{\rho}_p$ and radius $\ell$ as long as condition (19) holds together with the load being on the ground. The equations of motion at this state are [2]

$$\begin{bmatrix} \dot{\boldsymbol{\rho}}_q \\ \dot{\boldsymbol{v}}_q \\ \dot{\boldsymbol{R}} \\ \dot{\boldsymbol{\Omega}} \end{bmatrix} = \begin{bmatrix} \boldsymbol{v}_q \\ m_q^{-1}(\boldsymbol{R}\boldsymbol{F} - \mathcal{T}\boldsymbol{\mu}) - g\boldsymbol{z}_E \\ \boldsymbol{R}\boldsymbol{\Omega}_\times \\ \boldsymbol{I}_{x,y,z}^{-1}(-\boldsymbol{\Omega} \times \boldsymbol{I}_{x,y,z}\boldsymbol{\Omega} + \boldsymbol{\tau}) \end{bmatrix}. \tag{20}$$

– **Raise:**
The transition from *Pull* to *Raise* happens when the condition

$$\mathcal{T}(\boldsymbol{\mu}^T \boldsymbol{z}_E) > m_p g \tag{21}$$

holds, which means that the tension force is enough to lift the suspended load in the upwards direction. The load is now in the air with the cable completely taut (Fig. 3c). The equations of motion are now written in its full form given in (3), which gives

$$\begin{bmatrix} \dot{\boldsymbol{\rho}}_q \\ \dot{\boldsymbol{v}}_q \\ \dot{\boldsymbol{R}} \\ \dot{\boldsymbol{\Omega}} \\ \dot{\boldsymbol{\rho}}_p \\ \dot{\boldsymbol{v}}_p \end{bmatrix} = \begin{bmatrix} \boldsymbol{v}_q \\ m_q^{-1}(\boldsymbol{R}\boldsymbol{F} - \mathcal{T}\boldsymbol{\mu}) - g\boldsymbol{z}_E \\ \boldsymbol{R}\boldsymbol{\Omega}_\times \\ \boldsymbol{I}_{x,y,z}^{-1}(-\boldsymbol{\Omega} \times \boldsymbol{I}_{x,y,z}\boldsymbol{\Omega} + \boldsymbol{\tau}) \\ \boldsymbol{v}_p \\ m_p^{-1}\mathcal{T}\boldsymbol{\mu} - g\boldsymbol{z}_E \end{bmatrix}, \tag{22}$$

together with (19), (21) and $\boldsymbol{z}_p > 0$.

## 3 Method

The simulation environment used was a modified version of the quadrotor Simulink model from Peter Corke's Robotics Toolbox for MATLAB [10]. The quadrotor model parameters were the same as the ones provided in the package. For simplicity we will assume in the equations above that $\mathcal{T}$ is implemented in such a way that $\boldsymbol{\Omega} \equiv 0$ and $\boldsymbol{R}(t) = \boldsymbol{R}(t_0) = \boldsymbol{I}_{3\times 3},\ \forall\, t$.

### 3.1 Modelling tension

The way Cruz et al. [2] computes the cable tension $\mathcal{T}$ for each mode is unrealistic, since accelerations are often very hard to measure reliably, thus making it very hard to implement a control law for the cable tension $\mathcal{T}$. At the same time, the only state that benefits from tension control is the *Pull* state, i.e., when the tension $\mathcal{T}$ should reach a value enough to lift the suspended load from the ground.

To find the correct expression for approximating $\mathcal{T}$ in the *Pull* state, one realizes that this is the amplitude of the reaction force induced by the holonomic constraint

$$\|\boldsymbol{\rho}_q - \boldsymbol{\rho}_p\|^2 = \ell^2. \tag{23}$$

Differentiating this constraint with respect to time and using the fact that $\boldsymbol{v}_p = 0$ at the *Pull* state, one obtains

$$\boldsymbol{v}_q^T(\boldsymbol{\rho}_q - \boldsymbol{\rho}_p) = 0.$$

Differentiating one more time and using the product rule of differentiation we obtain

$$\dot{\boldsymbol{v}}_q^T(\boldsymbol{\rho}_q - \boldsymbol{\rho}_p) + \boldsymbol{v}_q^T\boldsymbol{v}_q = 0. \tag{24}$$

Substituting (10) and (11) into (24) one obtains

$$\dot{\boldsymbol{v}}_q^T\ell\boldsymbol{\mu} = -\|\boldsymbol{v}_q\|^2.$$

Multiplying the expression for $\dot{\boldsymbol{v}}_q$ in (20) by $\boldsymbol{\mu}^T$ (since $\boldsymbol{\mu}^T\boldsymbol{\mu} = 1$) one can get rid of $\dot{\boldsymbol{v}}_q$ and compute the expression for $\mathcal{T}$, which becomes

$$\mathcal{T} = \frac{m_q}{\ell}\|\boldsymbol{v}_q\|^2 + m_q\boldsymbol{\mu}^T\left(-g\boldsymbol{z}_E + \frac{1}{m_q}\boldsymbol{R}\boldsymbol{F}\right). \tag{25}$$

Just as the load starts lifting and the system enters *Raise* state, the equation above is no longer valid. To find the equation for the tension if $\boldsymbol{v}_p \neq 0$, one has to recompute the derivatives of the holonomic constraint in (23). Differentiating twice with the assumption that $\boldsymbol{v}_p \neq 0$ we have

$$(\dot{\boldsymbol{v}}_q - \dot{\boldsymbol{v}}_p)^T \ell \boldsymbol{\mu} = -\|\boldsymbol{v}_q - \boldsymbol{v}_p\|^2.$$

Computing $\dot{\boldsymbol{v}}_q - \dot{\boldsymbol{v}}_p$ from (22) with respect to $\mathcal{T}$ and substituting $(\dot{\boldsymbol{v}}_q - \dot{\boldsymbol{v}}_p)^T \ell \boldsymbol{\mu}$ for $-\|\boldsymbol{v}_q - \boldsymbol{v}_p\|^2$, one ends up with the following expression

$$\mathcal{T} = \frac{m_p}{m_q + m_p} \left( \mu^T \boldsymbol{R} \boldsymbol{F} + \frac{m_q}{\ell} \|\boldsymbol{v}_q - \boldsymbol{v}_p\|^2 \right). \tag{26}$$

In order to lift the payload, the total thrust $\boldsymbol{F}$ has to be increased in the direction of $\boldsymbol{z}_E$ such that the cable tension value $\mathcal{T}$ is above the load weight $m_p g$ [2]. The condition in (21) acts as an indication for the system to move over to the *Raise* state. There could also be a transition back from *Pull* to *Setup*, under which circumstances the condition $\mathcal{T} = 0$ has to be met [2].

To model the tension developed in a weighted cable in the general case, one may utilize the dynamics of a one-sided stiffness. A one-sided stiffness, or spring model, is a realistic approximation to actual cable behavior. According to Hooke's Law, the tension $\mathcal{T}$ is proportional to the relative stretch $s = \lambda/\ell$ in the cable, where $\lambda$ is the additional length to the cable of length $\ell$ when it is stretched such that $\hat{\ell} = \ell + \lambda$.

Modelling the tension force as a one-sided stiffness one obtains

$$\mathcal{T} = m_q \frac{k_e}{\ell} \lambda, \tag{27}$$

which is only valid when $\|\boldsymbol{\rho}_q - \boldsymbol{\rho}_p\| \geq \ell$. For the case when $\|\boldsymbol{\rho}_q - \boldsymbol{\rho}_p\| < \ell$, the tension is modelled to be $\mathcal{T} = 0$. $k_e$ is the stiffness (spring constant), which is used to describe the elasticity of the cable. For this case, $k_e$ is chosen to be quite high, i.e., the cable is not very elastic.

### 3.2 Trajectory control without a cable-suspended load

Since the dynamics are decoupled during *Setup* state, traditional trajectory control suffices to move the quadrotor along desired trajectories.

Based on a given initial position $\boldsymbol{\rho}_q^{(0)}$ and time $t_0$, and a final position $\boldsymbol{\rho}_q^{(f)}$ and time $t_f$, one can generate a set of cubic polynomial trajectories $\boldsymbol{\rho}^*(t) = [x^*(t),\ y^*(t),\ z^*(t)]$ and their derivatives $\boldsymbol{v}^*(t)$ and $\dot{\boldsymbol{v}}^*(t)$, which are continuous in $\mathbb{R}^3$ [11, p. 188].

These trajectories can be used as references for a trajectory controller to make the quadrotor track a given trajectory to a final destination with desired velocity and acceleracion. To achieve perfect tracking of the trajectory $\boldsymbol{\rho}_q^*(t)$, the following control law can be used [7]

$$\boldsymbol{F}_1 = m_q \boldsymbol{R}^T \left[ \dot{\boldsymbol{v}}_q^* + K_d \left( \boldsymbol{v}_q^* - \boldsymbol{v}_q \right) + K_p \left( \boldsymbol{\rho}_q^* - \boldsymbol{\rho}_q \right) + g \boldsymbol{z}_E \right], \tag{28}$$

with $K_p > 0$ and $K_d > 0$.

### 3.3 Trajectory & Tension control with a cable-suspended load

Since the equations (25)-(26) for computing the tension during *Pull* and *Raise* are merely theoretical because the holonomic constraint in (23) will almost never hold, one realizes that this can not be used for implementing a control law for tracking a trajectory while also maintaining a constant tension on the cable.

When the load lifts from the ground, the quadrotor will be affected by the dynamics of the cable-suspended load. By combining trajectory control in (28) together with a tension error term $\Lambda(\mathcal{T} - \mathcal{T}^*)\boldsymbol{\mu}$, where $\mathcal{T}^* = \hat{m}_p g(\boldsymbol{\mu}^T \boldsymbol{z}_E)$ is the desired tension and $\Lambda$ is a gain factor, one will achieve asymptotic tracking of a given trajectory despite the contradicting forces generated from the cable-suspended load. $\hat{m}_p$ is the estimated mass of the load, which is explained further in Section 3.5. The control law for *Pull* and *Raise* can be written as

$$\boldsymbol{F}_2 = \boldsymbol{F}_1 + \boldsymbol{R}^T \left[\mathcal{T} - \hat{m}_p \Lambda(\mathcal{T} - \mathcal{T}^*)\right] \boldsymbol{\mu}, \tag{29}$$

which is similar to impedance control in the simplest form [11, p. 330].

### 3.4 Implementing the lifting maneuver

Back to the problem of a quadrotor having to lift a cable-suspended payload, starting at an arbitrary position $\boldsymbol{\rho}_q^{(0)}$ within the half sphere with its center at $\boldsymbol{\rho}_p$ and radius $\ell$. The first action to be done is to have the quadrotor move straight above the payload such that

$$\|(x_q,\ y_q) - (x_p,\ y_p)\| = \|(e_{x,p},\ e_{y,p})\| = 0. \tag{30}$$

When (30) holds true, the system enters the *Setup* state. In the *Setup* state, the quadrotor increases its altitude until (19) holds true. These procedures can be done using trajectory control with the control law proposed in (28). When (19) holds, the system transitions into the *Pull* state. In *Pull* state, the quadrotor has to increase the tension force induced by the cable using TT control with the control law proposed in (29). When the tension is larger than the gravitational force acting on the payload, it will lift from the ground and the TT controller will maintain $\mathcal{T} = \mathcal{T}^*$ while also achieves perfect tracking of the trajectory.

In order for a system to make sense of the procedures described above, some mathematical model of computation has to be used. A finite state machine (FSM) has been developed in order to determine the state of the system at a particular moment based on measurements from a tension sensor, given that such a sensor exists. The proposed state machine is illustrated in Fig. 5.

Since different controllers are used depending on the state the system is in, the state machine has to select the controller to be used for a particular state. Using a signal $select \in \{0, 1\}$, one can choose whether to pass on the computed thrust $\boldsymbol{F}_1$ from the trajectory controller or $\boldsymbol{F}_2$ from the TT controller. The selected force $\boldsymbol{F}_{sel}$ can be computed as

$$\boldsymbol{F}_{sel} = (1 - select)\, \boldsymbol{F}_1 + select\, \boldsymbol{F}_2, \tag{31}$$

where the applied thrust to the system is $\boldsymbol{F} = \boldsymbol{F}_{sel}$.

Everything described in this chapter can be summarized in Fig. 4, which illustrates the conceptual control system that can be used to implement the lifting maneuver.

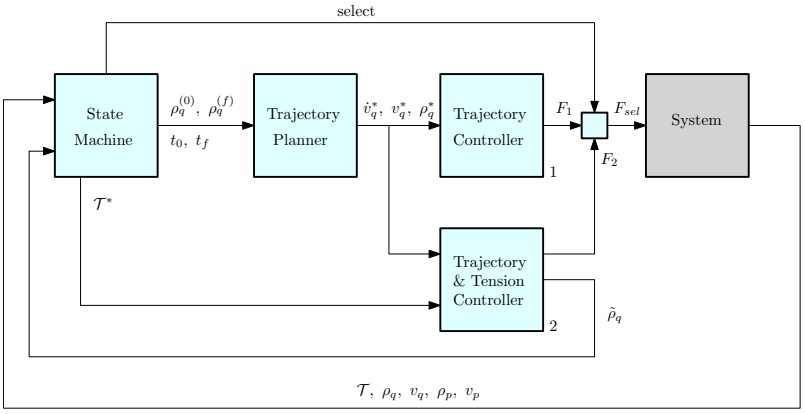


Fig. 4: A conceptual figure of the control system. Cyan blocks belong to the lifting maneuver implementation and grey blocks belong to the rest of the system. The system is assumed to be able to provide measurements of the value of $\mathcal{T}$.

### 3.5 Safety measures in the lifting maneuver

Attempting to lift a heavy payload is not necessarily dangerous if the aerial vehicle thinks the load is light. However, lifting a light payload while thinking the load is heavy could be fatal since the payload will most certainly sling up in the air hitting bystanders with potentially huge forces. As an extension to the lifting maneuver, safety measures have been implemented into the state machine which attempts to avoid the consequences of human error in the specification of the mass of the payload.

Another addition is a mass update routine which enables the system to adjust itself if the specified mass of the payload had been mislabeled. The update variable $\hat{m}_p$ is the estimation of the load mass with initial value $\hat{m}_p^{(0)} = m_p^*$ where $m_p^*$ is the first assumption of the mass of the load.

The first safety measure is to abort the lifting maneuver if the load seems unexpectedly light compared to what the system has been informed, denoted as *Abort Low*. To detect this, one realizes that the problem will arise when attempting to lift the payload at the instant when (19) holds true, i.e., the system is in the *Pull* state. One also realizes that if the load is too small and the system attempts to reach $\mathcal{T}(\boldsymbol{\mu}^T \boldsymbol{z}_E) > \hat{m}_p g$ before the payload lifts from the ground, the payload will actually clear from the ground before this condition

holds since $\hat{m}_p g > m_p g$. To detect this, one can look at the tracking error from TT Control to see if it is converging to zero, which means that the quadrotor follows the trajectory and is no longer influenced by the load. Denoting the tracking error as $\tilde{\boldsymbol{\rho}}_q = \boldsymbol{\rho}_q^* - \boldsymbol{\rho}_q$, it is said to have converged if

$$\|\tilde{\boldsymbol{\rho}}_q\| < \epsilon, \tag{32}$$

where $\epsilon$ is a sufficiently small value.

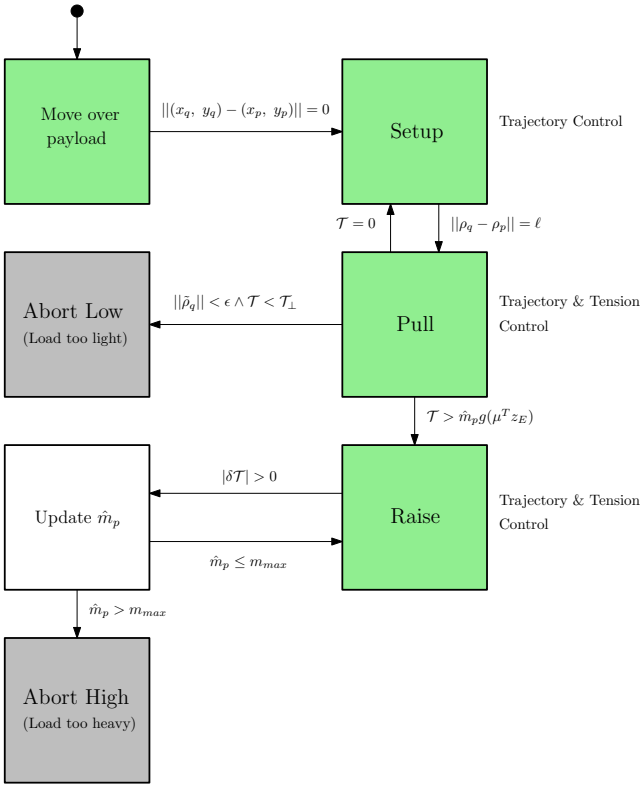


Fig. 5: The proposed state machine. The design takes inspiration from Cruz et al. [2], but is extended with appropriate safety measures and a load mass update routine.

Additionally, a lower bound for which the tension is acceptible when (32) holds true can be written as

$$\mathcal{T}_\perp = (1 - \sigma_\perp)\hat{m}_p g, \tag{33}$$

where $\sigma_\perp$ is a deviation variable to determine how much the bound should differ from the expected tension value.

If (32) holds true and $\mathcal{T} < \mathcal{T}_\perp$, the load is considered too light and the lifting maneuver will abort. The quadrotor will lower the load onto the ground and stop.

The second safety measure is to abort the lifting maneuver if the load mass exceeds the maximum cargo weight $m_{max}$ allowed by the quadrotor, denoted as *Abort High*. However, if the mass of the load is unexpectedly large compared to the assumed mass but is not exceeding $m_{max}$, the system will try to adjust the estimated load mass $\hat{m}_p$ until the tension on the cable is lower than the upper bound $\mathcal{T}_\top$ of the estimated mass. One realizes that the load may only be too heavy if the system has entered the *Raise* state since the tension will indeed be $\mathcal{T} > \hat{m}_p g$. Moreover, the mass is only considered too heavy if the estimated mass is

$$\hat{m}_p > m_{max}. \tag{34}$$

Before proceeding, we denote the relative error of the tension as

$$\delta\mathcal{T} = \frac{\mathcal{T} - \mathcal{T}^*}{\mathcal{T}^*}, \quad \mathcal{T} \geq 0, \quad \mathcal{T}^* \geq 0. \tag{35}$$

If the relative error of the tension is larger than zero, i.e., $\delta\mathcal{T} > 0$, the load is considered unexpectedly heavy compared to the estimated mass $\hat{m}_p$ and the system will attempt to estimate a new value of $\hat{m}_p$ to improve tracking of the trajectory controller. The update law for $\hat{m}_p$ is chosen to be

$$\hat{m}_p := \hat{m}_p + \alpha\,(\delta\mathcal{T}), \tag{36}$$

where $\alpha$ is the adjustable update gain. This will enable the estimated mass to be updated in the direction of the relative error of the tension, which means that $\hat{m}_p \to m_p$ as $\delta\mathcal{T} \to 0$ if we update $\hat{m}_p$ as long as $\delta\mathcal{T} > 0$, with a convergence rate determined by $\alpha$.

The safety measures proposed has been embedded into the FSM in Fig. 5.

## 4 Results

Implementing the system proposed in Section 3.4 and the safety measures proposed in Section 3.5 in a Matlab Simulink environment, one can verify the robustness and accuracy of the control laws and safety measures. We start with introducing the parameters used in Table 3.

To enable focus on the actual task, which is evaluating the proposed control laws and safety measures, the quadrotor was modelled as an approximative point mass with a constant orientation. This eased the time and effort required when constructing and running multiple test cases in the simulation environment.

The quadrotor starts at $\boldsymbol{\rho}_q^{(0)} = (1,\ 1,\ 2)$ and the load at $\boldsymbol{\rho}_p^{(0)} = (0,\ 0,\ 0)$. Though the following results will only investigate the performance of the system and safety measures during lifting; the quadrotor can start at an arbitrary position within a distance of the cable length from the load, and the results will be the same.

A video of simulations showcasing the safety measures has been made as supplementary material for this paper and is avaliable in [12].

| Parameter | Value | Method of acquisition |
|---|---|---|
| $m_q$ | 4 $kg$ | Robotics Toolbox |
| $m_p^*$ | 1 $kg$ | Intuition |
| $m_{max}$ | 2 $kg$ | $m_q/2$ |
| $\ell$ | 4 $m$ | Intuition |
| $\sigma_\perp$ | 0.1 | Intuition |
| $\epsilon$ | 0.001 | Intuition |
| $K_p$ | 16 | Tuning |
| $K_d$ | 8 | Tuning |
| $\Lambda$ | 10 | Tuning |
| $\alpha$ | 0.008 | Tuning |

Table 3: Parameters used during simulations.

### 4.1 Tracking error and convergence

We begin looking at the tracking error $|\tilde{\boldsymbol{\rho}}_q|$ at different $m_p$ where the initial assumption was $m_p^* = 1\ kg$. Simulations of the tracking error were made for five equisidant load masses $m_p$. The quadrotor attempts to track a trajectory while maintaining a constant tension on the cable attached between the quadrotor and the load. The result is presented in Fig. 6.

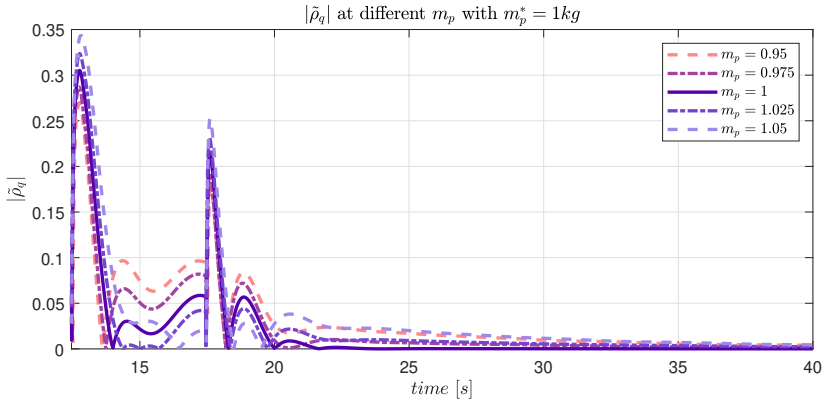


Fig. 6: The tracking error from the moment that the system has entered the *Raise* state until the end of the simulation. Five (5) tests with varying masses $m_p$ were performed and the resulting tracking error from each test is presesnted in the figure. The parameters used are found in Table 3.

During the *Raise* state, the system will attempt to estimate the true mass of the payload based on the relative error of the tension, $\delta\mathcal{T}$. The errors (residuals) between the true masses $m_p$ and the estimated masses $\hat{m}_p$ for five unique tests are presented in Fig. 7.

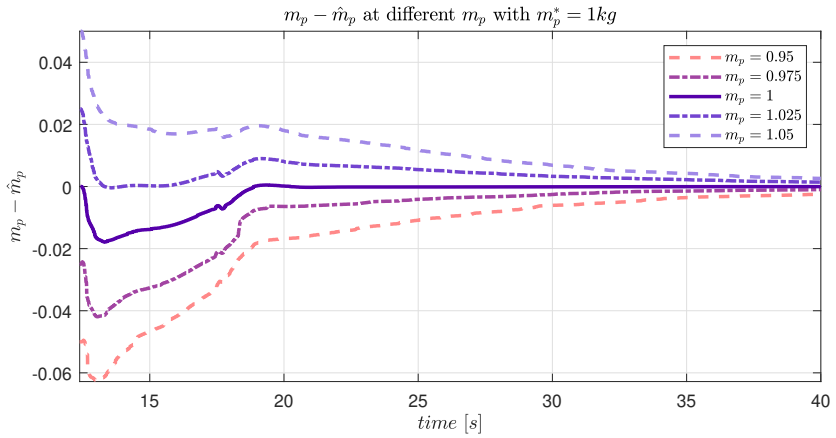


Fig. 7: The residual between the true mass $m_p$ and the estimated mass $\hat{m}_p$ for five (5) tests with varying masses $m_p$. The figure is focused on the interval of the moment that the system has entered the *Raise* state until the end of the simulation. The parameters used are found in Table 3.

The relative error bound $|\delta\mathcal{T}|$ of the tension has converge to zero to assume that the tension $\mathcal{T}$ on the cable is maintained such that $\mathcal{T} = \mathcal{T}^*$. This is done using the control law proposed in (29). The resulting relative error bound for five tests with different masses $m_p$ can be observed in Fig. 8.

### 4.2 Swing of the payload during lifting

For a lifting maneuver to be considered safe, the swing of the payload has to be minimal. Fig. 9 shows the distance between the quadrotor and the payload with cable length $\ell = 4\ m$ and the swing of the payload in the X-Y plane.

### 4.3 Robustness of safety measures

Safety measures will take over when either the load is unexpectedly too small (*Abort Low*) or if the maximum cargo weight $m_{max}$ is exceeded (*Abort High*). The point of switching between the *Raise* state and one of these modes has to be sufficiently robust to avoid unwanted behavior in the intervals of $m_p$ close to $(1 - \sigma_\perp)\hat{m}_p$ where the transition behavior is potentially unpredictable. Using the parameters in Table 3, the transition from *Raise* to *Abort Low* is detected in the interval $0.85 < m_p < 0.95$ and the transition from *Raise* to *Abort High* is detected in the interval $1.95 < m_p < 2.05$. A hundred (100) simulations using equisidant varying $m_p$ in the interval for each transition is presented in Fig. 10.

As can be observed in Fig. 10, there is an overlapping interval between *Raise* and *Abort Low* measured at $[0.9,\ 0.92]$ where the transition between the states is unpredictable.

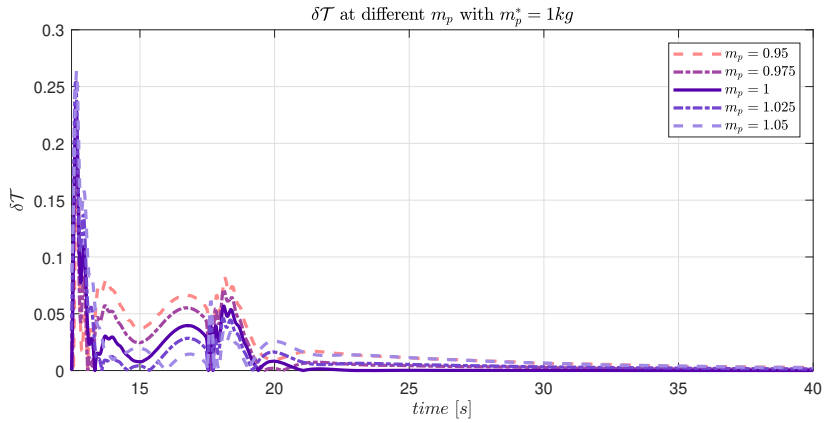


Fig. 8: The relative error bound of the tension during the *Raise* state where the system attempts to maintain a constant tension on the cable such that $\mathcal{T} = \mathcal{T}^*$. Tests were made for five (5) varying masses $m_p$. The parameters used are found in Table 3.

## 5 Discussion

The tracking error of the system following a trajectory in *Raise* state seems to converge to zero, which means that we achieve perfect tracking at some point during lifting of the cable-suspended load. This was observerd in Fig. 6. The tension during *Raise* appears to be maintained at the desired value since the relative error bound in Fig. 8 converges to zero quite rapidly. The load mass estimation error in Fig. 7 seem to also converge to zero which means that the system sucessfully estimates a value of the load mass close to the true value.

The swing of the cable-suspended load during lifting seem to be minimal, as can be observed in Fig. 9. Despite the tension on the cable is modelled as a stiff one-sided spring, there is still going to be some flex present, which can be observed in the steady state value of the distance between the UAV and the suspended load not being exactly equal to the cable length.

As can be observed in Fig. 10, the transition between *Raise* to *Abort High* seems to be quite robust since there are minimal overlapping of the $m_p$ logged in *Raise* and the $m_p$ logged in *Abort High*. There is a significant overlapping interval between *Raise* and *Abort Low* in which the transition is deemed unpredictable and the user should be aware of this unrobust interval.

### 5.1 Future work

A valid route for research could be to analyze the use of the expressions for tension derived from the holonomic constraint in (23) for aiding tracking in the trajectory control during lifting. Another desire for development would be to derive the dynamics using generalized coordinates, which in theory would greatly

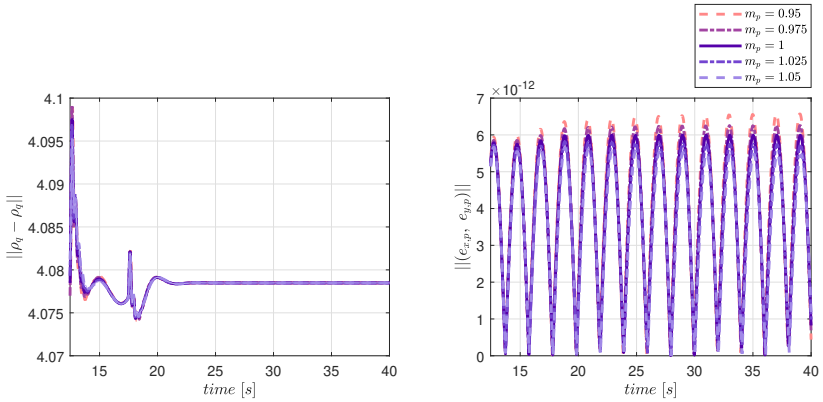


Fig. 9: To the left is the distance between the quadrotor and the payload during the *Raise* state. To the right is the swing of the payload in the X-Y plane during the same time. Tests were made for five (5) varying masses $m_p$. The parameters used are found in Table 3.

improve numerical reliability and would potentially allow holonomic constraints to be used.

A better method for determining the transition condition from *Raise* to *Abort Low* should be investigated further to increase robustness around the transition point or at least decrease the overlapping interval observed in Fig. 10.

In this paper, the control law in (29) was not proven to be asymptotically stable. Due to time limits there was no time to investigate this further, but a suggestion is to use the tension modelled as a one-sided stiffness to design a Lyapunov function candidate that provides a control law similar to (29) and guarantees global asymptotic stability according to La'Salle's theorem.

## 6 Conclusions

The safety measures proposed in Section 3.5 seem to be valuable additions to the hybrid automata proposed by Cruz et al. [2]. Moreover, true expressions for the tension have been derived. Cruz et al. [2] discusses the desire of performing the lifting maneuver with unknown mass, which has been done in this paper to some extent. The proposed update law for adjusting estimated mass for small deviations of the true mass of the payload has shown to be a reasonable choice when the mass is—not unknown—but unexpectedly different to the assumed mass.

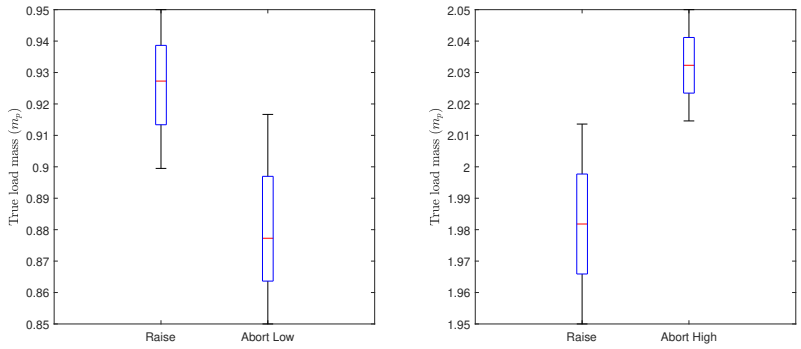


Fig. 10: To the left, a box plot of the transition between *Raise* and *Abort Low*. To the right, a box plot of the transition between *Raise* and *Abort High*. A hundred (100) simulations using equisidant varying $m_p$ were performed in the intervals specified in the vertical axis of each plot. The parameters used are found in Table 3.

## Acknowledgement

We thank Leonid Freidovich for assistance and comments that greatly improved the quality of this project.

## References

[1] Wallar, A., Plaku, E., Sofge, D.A.: Reactive motion planning for unmanned aerial surveillance of risk-sensitive areas. IEEE Transactions on Automation Science and Engineering **12**(3) (2015) 969–980

[2] Cruz, P., Fierro, J.: Cable-suspended load lifting by a quadrotor uav: hybrid model, trajectory generation, and control. Autonomous Robots **41**(8) (2017) 1629–1643

[3] Dai, S., Lee, T., Bernstein, D.: Adaptive control of a quadrotor uav transporting a cable-suspended load with unknown mass. In: Proceedings of the IEEE Conference on Decision and Control, 2015(February). (2014) 6149–6154

[4] Michael, N., Fink, J., Kumar, V.: Cooperative manipulation and transportation with aerial robots. Autonomous Robots **30**(1) (2011) 73–86

[5] Palunko, I., Fierro, R., Cruz, P.: Trajectory generation for swing-free maneuvers of a quadrotor with suspended payload: A dynamic programming approach. In: Robotics and Automation (ICRA), 2012 IEEE International Conference on. (2012) 2691–2697

[6] Association, C.S.: Helicopter lifting. Ontario: Safety guidelines for construction (2000)

[7] Mahony, R., Kumar, V., Corke, P.: Multirotor aerial vehicles: Modeling, estimation, and control of quadrotor. Robotics & Automation Magazine, IEEE **19**(3) (2012) 20–32

[8] Bouabdallah, S., Murrieri, P., Siegwart, R.: Towards autonomous indoor micro vtol. Autonomous Robots **18**(2) (2005) 171–183
[9] Bisgaard, M., Bendtsen, J.D., Cour-Harbo, A.L.: Modeling of generic slung load system. Journal of Guidance, Control, and Dynamics **32**(2) (2009) 573–585
[10] Corke, P.: Robotics, Vision & Control. Springer (2017)
[11] Spong, M., Hutchinson, S., Vidyasagar, M.: Robot modeling and control. Hoboken, N.J.: Wiley (2006)
[12] Söderlund, H.: Safety measures for vtol uav lifting a cable-suspended load with unexpected mass. Youtube (2018) `https://www.youtube.com/watch?v=7zBszVhinlc`, accessed 2018-12-15.